Statistical determinants of visuomotor adaptation in a virtual reality three-dimensional environment

E. Ferrea[1]*, P. Morel[1,4]*, J. Franke[1,2], A. Gail[1,2,3]

1 German Primate Center, Sensorimotor Group, Goettingen, Germany,
2 University of Goettingen, Georg-Elias-Mueller Institute of Psychology, Goettingen, Germany,
3 Bernstein Center for Computational Neuroscience, Goettingen, Germany
4 Univ. Littoral Côte d'Opale, Univ. Lille, Univ. Artois, ULR 7369 - URePSSS - Unité de Recherche Pluridisciplinaire Sport Santé Société, F-59140 Dunkerque, France

*equal contribution

Corresponding author: eferrea@dpz.eu

Abstract

Recent advances in virtual reality (VR) technology allow motor control studies to investigate movement variety in a controlled 3D environment. However, visuomotor adaptation paradigms for arm reaches in a 3D space are still scarcely investigated. Elucidating these adaptations is important to further our understanding, predicting and hence, rehabilitating everyday movement behavior in humans suffering from motor deficits. We test how well optimal integration theory that was extrapolated from 1D and 2D settings extends to movements in 3D space; specifically, if and how a subject's variability in planning and sensory perception will influence motor adaptation. We test this hypothesis without introducing artificial (experimentally induced) variability. Instead, we exploit the natural anisotropy in sensory performance along different dimensions relative to the body. We use a virtual reality (VR) setup to compare the subject's adaptation of their 3D movements to perturbations applied separately in sagittal, coronal and horizontal planes. We found that subjects adapt best to perturbations in the coronal plane, i.e. when the depth component of the movement is unaffected, followed by sagittal then horizontal perturbations. To characterize how the adaptation rate selectively depends on planning and sensory uncertainty along different body axes, we developed a novel hierarchical two-state space model using Bayesian modeling via Hamiltonian Monte Carlo procedures to fit visuomotor adaptation profiles. Our

hierarchical model reconstructs learning parameters from surrogate data better than a state-of-the-art expectation-maximization (EM) algorithm. Modeling revealed that differences in adaptation rate of movement among the three planes are explained from the Kalman gain, i.e. the relative variability associated with planning and sensory perception. The developed method allowed us to show that the motor behavior is in line with optimal integration theory when considering adaptation rate variation between the different planes.

Author Summary

The process of neurorehabilitation in human patients suffering from motor deficits could be considered as a process of relearning or re-adapting motor skills. Virtual reality is already used to drive motor rehabilitation. However, the majority of motor learning theories were developed under one or two-dimensional experimental paradigms and it is assumed that the general findings apply to motor control in three-dimensional movements. To test whether these theories are also compatible with more naturalistic movements performed in a three-dimensional space, we used a new statistical method to identify the dynamics of motor adaptation in virtual reality. We found that in a three-dimensional environment, there are differences in how the subject will correct and adapt their movement based on which orientation relative to the body the movement needs to be corrected. These differences come from the statistical variability associated with unperturbed movements in the different directions. These findings provide clues on how therapeutic regimens in virtual reality should be adapted, i.e. physical reorientation of the body, to improve rehabilitation of certain movements.

Introduction

Research on visuomotor adaptation of limb movements is mostly performed in one or two-dimensional reach-movement settings (Mazzoni and Krakauer 2006, Krakauer 2009, Wolpert, Diedrichsen et al. 2011,

56 Taylor, Krakauer et al. 2014, McDougle, Bond et al. 2015, Morehead, Qasim et al. 2015, Leow, de Rugy
57 et al. 2016). However, these theories, still need to be tested in less constrained 3D settings (Anglin,
58 Sugiyama et al. 2017). It is unknown, for example, if and how spatial anisotropy in sensory perception
59 translates into motor adaptation anisotropy. Here, we test the prediction of optimal integration (OI)
60 theory that natural variability in sensory measurement between different dimensions relative to the
61 body determines the corresponding motor adaptation rates (Scott 2004, Shadmehr and Krakauer 2008,
62 Diedrichsen, Shadmehr et al. 2010, Shadmehr, Smith et al. 2010, Friston 2011).

63 Virtual reality (VR) setups allow humans to perform a rich variety of movements in controlled 3D
64 experimental conditions (Choi, Lee et al. 2018) and can be flexibly used in laboratory settings to test
65 motor control theories. Among these theories, OI theory is the dominant principle to explain motor
66 adaptation. It proposes that the nervous system, according to a specified goal, optimally combines visual
67 and proprioceptive information with a forward prediction of the body's state (Wolpert and Ghahramani
68 2000, Ernst and Banks 2002, van Beers, Baraduc et al. 2002, Kording and Wolpert 2004) to control
69 movements and to correct errors. During motor adaptation, this forward model is updated to reduce the
70 sensory prediction error arising from a mismatch between its prediction and the sensory feedback.
71 Variability in sensory feedback or other variability in this closed-loop process thus affects the observed
72 rate of adaptation.

73 Variability arises due to the stochastic nature of neuronal processes in the sensorimotor transformations
74 (i.e., the planning and execution of the movement), referred to as "planning variability", and directly
75 affects the reliability of the forward model prediction (Korenberg and Ghahramani 2002, Cheng and
76 Sabes 2006, Cheng and Sabes 2007, van Beers 2009, Morel and Baraduc 2010). Other sources of
77 variability are directly attributed to the visual or proprioceptive feedback and affect the estimate of the

effector position (hereafter “measurement variability”) (Kording and Wolpert 2004, Burge, Ernst et al. 2008, Wei and Kording 2010).

According to OI theory, during adaptation, a statistically optimal solution for the update of the forward model is the Kalman filter (Kalman 1960), where corrections are weighed by the measurement variability and planning variability (Ghahramani, Wolpert et al. 1997, Baddeley, Ingram et al. 2003, Burge, Ernst et al. 2008). Higher variability in the forward model (high planning variability) would increase the Kalman gain and allow faster corrections of the experienced error, whereas a higher variability in the sensory feedback (high measurement variability) would determine a lower gain and therefore a slower adaptation. Previous studies found that human behavior approaches that of an optimal learner (Burge, Ernst et al. 2008, Wei and Kording 2010, He, Liang et al. 2016, van der Vliet, Frens et al. 2018) showing that adaptation rate positively correlates with the Kalman gain calculated from the planning and measurement variabilities. Recently, it was found that individual differences in the rate of motor adaptation are largely explained by individual differences in the Kalman gain (van der Vliet, Frens et al. 2018).

Here, we ask if adaptation in a three-dimensional space simulated in a virtual reality environment would still reflect an optimal learner model. Importantly, we aim to confirm these models by leveraging the existing differences in sensorimotor variabilities in the different planes of space, without needing to introduce artificial variability (van Beers, Sittig et al. 1999, Wei and Kording 2010).

Current experiments and models propose that sensorimotor adaptation is supported by two learning processes, which act on different timescales: one fast adapting and fast forgetting and one slow adapting and slow forgetting (Smith, Ghazizadeh et al. 2006, Wolpert, Diedrichsen et al. 2011). Compared to one-state models (Cheng and Sabes 2006, Cheng and Sabes 2007, van Beers 2009), two-state models explain motor adaptation as a combination of explicit and implicit learning mechanisms,

where explicit learning allows fast adaptation and implicit learning changes performance more slowly (Taylor, Krakauer et al. 2014, Huberdeau, Krakauer et al. 2015, McDougle, Bond et al. 2015). Two-stage models better explain phenomena like savings (improved learning due to repeated exposure) (Krakauer, Ghez et al. 2005, Huang, Haith et al. 2011, Avraham, Morehead et al. 2020) and anterograde interference (negative influence of past learning on future learning, (Sing and Smith 2010, Leow, de Rugy et al. 2016) that were found to be partially correlated with explicit learning (Morehead, Qasim et al. 2015). Moreover, neurophysiological evidence of two-state learning dynamics was found in humans and monkeys (Della-Maggiore, Malfait et al. 2004, Inoue and Kitazawa 2018). We fit fast- and slow-state processes during sensorimotor adaptation (Smith, Ghazizadeh et al. 2006) to estimate the adaptation rates. By considering the stochastic nature of error-based learning, we can independently estimate the measurement and planning uncertainty from the empirical movement data during a 3D adaptation task, with different perturbation planes oriented differently relative to the body. Stochastic modeling has been shown to better identify the time course of the hidden states (Albert and Shadmehr 2018). We used Bayesian inference via Hamiltonian Markov chain Monte Carlo sampling (referred to as Hamiltonian Monte Carlo, HMC) to implement a novel multilevel hierarchical version of the two-state space model fitting. We evaluated the hierarchical model and compared it to another state-of-the-art model performing Bayesian inference via an expectation-maximization (EM) algorithm (Albert and Shadmehr 2018) without a hierarchical structure. We show that HMC allows for a better extraction of data on the two underlying motor learning states and the planning and measurement variabilities. Using hierarchical HMC models, we confirm that two-state models better explain our experimental three-dimensional data than single-state models. We, therefore, use the two-state hierarchical HMC model to test whether differences in adaptation dynamics can be found between movements and perturbations of different directions relative to the subject's own body and whether these differences comply with OI theory.

Materials and Methods

Subjects

Data were collected from 26 healthy subjects (age range 20-32, 10 females, 16 males). The study was performed under institutional guidelines for experiments with humans, adhered to the principles of the Declaration of Helsinki, and was approved by the ethics committee of the Georg-Elias-Mueller-Institute for Psychology at the University of Goettingen. All the subjects were right-handed, had normal or corrected-to-normal vision and received financial compensation for their participation. Subjects gave written consent to participate and received detailed written instructions for the task. They were asked to paraphrase the instructions in their own words to make sure they understood the task. The experiment was carried out in one single appointment that lasted between 2.5 and 3 hours, depending on the subjects' freely chosen breaks among blocks (see later).

Virtual Reality Setup

Subjects sat in a darkened room (all distractions and light were removed). The temperature was ambient, there was no noise, the 26 experiments were done individually at different times of the day and on different days. Visual displays on two monitors were controlled by a customized C++ software similar to what was described in previous studies (Morel, Ferrea et al., 2016, Morel, Ulbrich et al., 2017). The images of the two monitors (one for each eye, BenQ XL2720T, 27-inch diagonal, 1920x1080, 60 Hz refresh rate, BenQ, Taepei, Taiwan) were reflected by two semi-transparent mirrors. (75 x 75 mm, 70/30 reflection/transmission plate beamsplitter, covered from the back to block transmission; stock #46-643, Edmund Optics Inc., Barrington, New Jersey, United States) that were angled 45° relative to the two monitors on each side of the subject (Fig. 1A). The two screens render a three-dimensional view of virtual objects on a dark background. To accommodate test subject ergonomy, we tilted the monitors downward by 30°. This ensured that arm movements in the physical space could be carried out in an

ergonomic posture in front of the body while the virtual representation (the cursor) of the hand was still aligned with the actual hand position and the virtual cube centered on the axis of gaze.

In the rest of the paper, we describe orientation relative to the tilted head of the subject and workspace, not according to true horizontal and vertical. To optimize the perception of the virtual workspace for each subject, the inter-pupillary distance was measured (range:51 to 68 mm, mean = 59.48 mm) and the 3D projection was modified in the custom-made software accordingly. This has been shown to benefit depth perception, reduce image fusion problems and reduce fatigue in participants (Rosenberg 1993).

Subjects performed controlled arm movements in the 3D environment. For this, they moved a robotic manipulator (delta.3, Force Dimension, Nyon, Switzerland) with their dominant hand to place the 3D cursor position into visual target spheres. The manipulator captured the hand position at (sampling frequency = 2 kHz with a 0.02 mm resolution). Since subjects could neither see their hand nor the robot, a cursor (yellow sphere, 6 mm diameter) indicated the virtual representation of the robot handle and therefore the hand position (Fig1B).

Behavioral task

Subjects performed a reaching-out task from a central fixation point to one of eight potential target positions (grey sphere, 25 mm diameter) arranged at the vertices of a 10 cm-sided cube centered on the fixation point (Fig. 1B-C). Each subject completed three blocks with breaks in between. One block consisted of 600 successful trials: 120 baseline trials, then 240 perturbed trials, and 240 washout trials again without a perturbation (Fig. 1D). Each block lasted between 20 to 25 minutes, depending on the performance of the subject. Breaks between blocks were adjusted according to the subject's needs and usually lasted between 10 to 15 minutes. Before the actual experiment, a short training session was run

170 to make subjects comfortable with the three-dimensional environment and to ensure a correct
171 understanding and execution of the task.

172 At the beginning of each trial, subjects moved the cursor (co-localized with the hand position) into the
173 central fixation sphere (semitransparent grey, 25 mm diameter) and held the cursor there for 200 ms
174 ("hold fixation"; Fig. 1B). After this holding period, one of the eight potential targets (grey, 8 mm
175 diameter) was briefly highlighted by a spatial cue (semitransparent grey sphere of 25 mm diameter,
176 centered on the target). The corners of the cube, and hence also the target, remained visible after the
177 cue stimulus disappeared to allow precise localization of the target in the 3D space. The size of the
178 spatial cue corresponded to the eligible area in which the movement had to end to be considered
179 successful. The spatial cue remained visible for 300 ms and then disappeared together with the fixation
180 sphere. This disappearance served as a GO signal for the subjects. Subjects then had 500 ms time to
181 leave the central fixation point and begin their hand movement towards the target. For successful
182 completion of the trial, it was sufficient that the cursor completely entered the target sphere, without
183 the need to stop inside the eligible area. Success or failure was indicated by sound signals: high-pitch for
184 success, low-pitch for failure. A trial was aborted if subjects had not left the starting point 500 ms after
185 the GO signal, if the movement was stopped (speed below 3cm/s) at any point outside the target area or
186 lasted longer than 10 seconds. After each trial, subjects could immediately start a new trial by moving
187 the cursor back to the starting position.

188 Within each block, we applied a 2D visuomotor perturbation to the 3D position of the cursor, i.e. a
189 perturbation which affected the cursor position sequentially to the xy-coordinate and then to the yz- or
190 xz-coordinates, respectively. For every perturbation, one out of the three dimensions was left
191 unperturbed, corresponding to the axis of rotation for the perturbation. In the perturbed trials, the
192 workspace was rotated by 30 degrees counterclockwise around either the x (rotation in the sagittal

193 plane), y (rotation in the horizontal plane) or z (rotation in the coronal plane) axes in each of the three
194 blocks (Fig. 1D). The rotation was applied in each block to one of the three planes. As proof of concept,
195 we verified that the projections of the trajectories on the perturbed planes look similar (Fig. 2A). The
196 order of the blocks (perturbation types) and thereby the rotated axes were controlled over the
197 experiment using stratified randomization between subjects. This should prevent potential effects of
198 fatigue or interference between blocks.

199 In both blocks, the subjects conducted the same movements in terms of starting and end positions. We
200 chose the corners of a cube as targets since any movement from the center of the cube to a corner
201 always is a diagonal movement that is composed of equally large x-, y- and z-components. Therefore,
202 the same target movement can be subjected to perturbations in each of the three planes parallel to the
203 surfaces of the cube. This allowed us to compare perturbations in different body-centered dimensions
204 without changing movement start and end positions, thereby avoiding potentially confounding effects
205 of posture.

206 Within each block of trials, the order of the targets was pseudo-randomized such that all eight targets
207 were presented within each set of eight successful trials. These 8-trial sets counted as epochs and the
208 model fitting analysis was carried out on epochs rather than on single trials.

209 **Data preprocessing**

210 Hand position data was acquired by sampling the manipulator position at 2 kHz and stored for offline
211 analysis performed in MATLAB® R2018a (MathWorks, Inc., Natick, Massachusetts, United States). Data
212 plots were generated with gramm, a MATLAB plotting library developed by the first co-author (Morel
213 2018). Trajectories were aligned in time from the start of the movement, defined as a speed increase
214 above 3 cm/s, to when the hand reached the target, and resampled in 50 time steps so that each
215 trajectory was normalized in duration.

To calculate the spatial deviation of the hand position for each perturbed plane independent of target direction, the trajectory of each trial was projected on the axis orthogonal to the center-to-target direction and laying in the plane of the applied perturbation (Fig. 2B, perturbed dimension). For each subject, each trajectory and each specific block, the mean baseline trace was subtracted to each trajectory to remove any trajectory bias (non-straight movements). Figure 2C (middle and bottom panel) shows, for one example subject, the average of the projected trajectories at baseline, during the first 8 trials (early adaptation) and the last perturbation trials (late adaptation) for all three perturbed planes. For our analysis, we considered the angle at half of the trajectory (Fig. 2C) that is indicative of the intended direction, which we expect to change over the course of adaptation.

Fitting model and procedure

Existing tools for fitting adaptation models (Albert and Shadmehr 2018, van der Vliet, Frens et al. 2018) can only estimate parameters from single experimental runs (changes over repeated trials in one task condition and one subject) despite the often hierarchical nature of the experiment (repeated trials interleaved with multiple conditions, multiple subjects). This is particularly problematic for two-state models due to their low identifiability (see results).

To get more reliable estimates of subject-level and population-level learning parameters, we developed a hierarchical-model version of single-state and two-state models of adaptation. For this, we used the probabilistic programming language Stan (Gelman, Lee et al. 2015), through its MATLAB interface. Stan allowed us to perform Bayesian inference with its implementation of a Hamiltonian Markov chain Monte Carlo using a NUTS sampler algorithm (Hoffman and Gelman 2014).

The underlying trial-by-trial adaptation model for the movement angle corrections is the following. For the trial n in subject j and perturbation plane p, the measured movement angle $y_{jp}(n)$ is:

$$y_{jp}(n) = x_{jp}(n) + \varepsilon_{u,jp}(n) \quad (1)$$

With $x_{jp}(n)$ being the hidden internal state (aiming angle) and $\varepsilon_{u,jp}(n)$ the measurement noise of the movement due to limited sensory accuracy of the agent, described by a normal distribution with zero mean: $\varepsilon_{u,jp}(n) \sim N(0, \sigma_{u,jp})$. The internal state depends on the previous state, with retention **A**, and the error e at the previous trial, with learning rate **B**. The state update is affected by a planning noise (or state update error) $\varepsilon_x(n)$, which gives us the following:

$$x_{jp}(n+1) = A_{jp}x_{jp}(n) + B_{jp}e_{jp}(n) + \varepsilon_{x,jp}(n) \quad (2)$$

In the single-state model, $A_{jp}$and B_{jp} are positive scalars, and $\varepsilon_{x,jp}(n) \sim N(0, \sigma_{x,jp})$. For the two-state model:

$$A_{jp} = \begin{bmatrix} a_{s,jp} & 0 \\ 0 & a_{f,jp} \end{bmatrix} \text{ with constrains } a_{s,jp} > a_{f,jp} > 0$$

$$B_{jp} = \begin{bmatrix} b_{s,jp} \\ b_{f,jp} \end{bmatrix} \text{ with constrains } b_{f,jp} > b_{s,jp} > 0$$

$$\varepsilon_{x,jp}(n) \sim N\left(\begin{bmatrix}0\\0\end{bmatrix}, \begin{bmatrix}\sigma_{x,jp} & 0\\ 0 & \sigma_{x,jp}\end{bmatrix}\right)$$

In our mixed-model, all subject and plane-level parameters: $\sigma_{u,jp}$, $a_{s,jp}$, $a_{f,jp}$, $b_{s,jp}$, $b_{f,jp}$, $\sigma_{x,jp}$ were drawn from population-level normal distributions, e.g. for $a_{s,jp}$ we define $a_{s,jp} \sim N(\mu_{a_s,p}, \sigma_{a_s})$. Here, $\mu_{a_s,p}$ and σ_{a_s} are population-level hyper-parameters, corresponding to the population (between-subject) average of the slow retention for perturbation plane p and the population standard deviation of the slow retention.

To keep the model simple, we did not include common per-subject offsets in the average hyper-parameters across planes; in other words, the model we used did not take into account the fact that the same subjects participated in experimental runs with different perturbed planes. A variation of the model which permitted per-subject offsets yielded equivalent results (data not shown).

Bayesian inference requires priors for the hyper-parameters, which were chosen wide to not constrain the model. Retention average hyper-parameter ($\mu_{a_s,p}$, $\mu_{a_f,p}$ in the two-state model and $\mu_{A,p}$ in the single-state model) priors were $\sim N(0,9)$, learning rate average ($\mu_{b_s,p}$, $\mu_{b_f,p}$ and $\mu_{B,p}$) priors were $\sim N(1,9)$, and their population standard deviation hyper-parameter ($\sigma_{a_s}, \sigma_{a_f}, \sigma_{b_s}, \sigma_{b_f}$ and σ_A, σ_B) priors were half-Cauchy distributions (location = 0, scale = 5) (Gelman 2006). Priors of the population average and standard deviation hyper-parameters of the measurement and planning noise ($\mu_{\sigma_x,p}, \mu_{\sigma_u,p}$ and $\sigma_{\sigma_x}, \sigma_{\sigma_u}$) were half-Cauchy distributions (location = 0, scale = 15). The conclusions from the model fitting do not critically depend on the exact choice of any of these parameters.

Steady-state Kalman gain

From the variances of the noise processes, we calculated the steady-state Kalman gain, as derived by Burge and colleagues (Burge, Ernst et al. 2008). In short, by introducing the term:

$$\sigma^2_{X_t^+} = \frac{-\sigma_x^2+\sqrt{(\sigma_x^2)^2+4\sigma_x^2\sigma_u^2}}{2} \qquad (4)$$

The Kalman gain (K) is calculated as follow:

$$K = \frac{\sigma^2_{X_t^+} + \sigma_x^2}{\sigma^2_{X_t^+}+\sigma_u^2+ \sigma_x^2} \qquad (3)$$

Validation of fitting procedure

To validate our hierarchical Bayesian fitting procedure, we compared it to non-hierarchical fitting procedures applied to surrogate data sets. For this, we generated N = 100 artificial experimental runs using the two-state model with the same number of baseline, perturbation, and washout trials as in our experiment. For each simulation, each parameter was drawn from a random normal distribution approaching the values we observed in our data (table 1). We then compared the accuracy of parameter estimations from different models, namely an EM algorithm (Albert and Shadmehr 2018) and a non-hierarchical and a hierarchical HMC model.

Table 1

Random parameter distributions

$$a_s \sim N(0.93, 0.03)$$

$$a_f \sim N(0.55, 0.2)$$

$$b_s \sim N(0.06, 0.04)$$

$$b_f \sim N(0.18, 0.08)$$

$$\sigma_x \sim N(1.5, 1)$$

$$\sigma_u \sim N(6, 3)$$

Table 1. Distributions of parameters in the surrogate data approaching the values observed in the experiments.

Results

The subjects performed the task (three conditions: baseline, perturbation and washout) with a high success rate in all perturbed planes (number of correct trials/number of total trials during movement phase > 99%). A generalized linear mixed effect model with a binomial distribution was used to test the effect of the perturbation in the different planes (fixed effect) on the success rate with the subjects as random effect. With the sagittal plane as intercept, there was no significant effect on the slope for the horizontal plane (tstat = 1.5477, p = 0.1217) and no significant effect for the slope of the coronal plane (tstat = 1.3976, p = 0.16223).

To test differences among the level of adaptation reached by the subjects, a one-way between-subjects ANOVA was conducted to compare the effects of the perturbed plane over the final adaptation level (calculated as the average of the adaptation profile over the last 4 epochs). We found that the subjects adapt differently to the perturbations depending on the plane of rotation. The final level of adaptation

304 was significantly higher for perturbations in the coronal plane compared to the sagittal plane (pcor-sag =
305 7.6E-05) and horizontal plane (pcor-hor = 1.0 E-08) (Fig. 3A). Moreover, perturbations in the sagittal
306 plane provide stronger adaptation than perturbations in the horizontal plane (psag-hor = 0.004) (Fig.
307 3A).

308 To understand the underlying dynamic of the differences in adaptation, we modeled adaptation behavior
309 in the three different visuomotor perturbation planes with a two-state model, which separately
310 identified the slow and fast processes underlying adaptation. While our hierarchical Bayesian model fits
311 data across conditions and subjects (see Methods), Figure 3B shows the fitted curves for one example
312 subject performing one adaptation condition. We also evaluated whether in such a three-dimensional
313 task, a two-state model fits the data better than a single-state model. The single-state model shows
314 larger root-mean-square residuals when subtracting the modeled adaptation trajectory from the
315 observed trajectory (Fig. 3C, paired t-test, p = 6.6e-16). To take into account the number of free
316 parameters when comparing models, we additionally computed the widely applicable information
317 criterion (WAIC), an approximation of cross-validation for Bayesian procedures (Vehtari, Gelman et al.
318 2017). The two-state model shows a lower WAIC compared to the single-state model (3.54E+04 and
319 3.58e+04, respectively), confirming a better fit of the two-stage model.

320 To validate our new hierarchical fitting procedure, we tested whether model parameters are better
321 reconstructed by our two-state Bayesian HMC hierarchical model compared to a state-of-the-art EM
322 algorithm (Albert and Shadmehr 2018). We also compared the HMC hierarchical model with the
323 corresponding non-hierarchical HMC model. For this, we generated surrogate adaptation datasets from
324 multiple two-state models with randomly sampled parameters (see Methods) and used the three
325 algorithms to retrieve the randomly sampled parameters. The hierarchical model better reconstructs all
326 parameters (error is smaller and correlation is higher)(Fig. 4).

Optimal integration theory (OI) predicts that the rate of adaptation correlates with the weighing between internal estimation and external sensory information for assessing the state of the system. A learner optimally integrating these two types of information approximates a Kalman filter that combines them depending on their respective uncertainties (variabilities). If planning (internal estimate) variability is high and measurement (sensory information) variability low during adaptation, the experienced error will be given credibility, and therefore faster learning will happen. In the opposite case, the learner tends to disregard the experienced error and corrections would happen slowly. To test if this mechanism can explain the observed differences between the perturbed planes in our experiment, we correlated planning noise and measurement noise variabilities with the slow learning rate Bs for each experimental run in our dataset (Fig. 5B).

Correlations between planning noise and the learning rate as well as between measurement noise and learning rate were low (respective R2 : 0.13 and 0.11), but with a trend consistent to the OI predictions, i.e. low measurement noise and high planning noise correlate with higher slow learning rate. When combining the contribution for each subject of the two noises into an estimate of a Kalman gain, the slow learning rate was explained much better (R2 between K and Bs : 0.48), with a high Kalman gain being associated with high learning rate (Fig. 5B, right). Notably, this relationship between Kalman gain (K) and slow learning rate (Bs) is only created by the different average values for K and Bs between the perturbation planes. This means, the slow learning rate is mostly explained by the plane of the workspace in which the perturbation is applied (R2 = 0.94), while it does not correlate with the Kalman gain variation across the individual subjects within a perturbation condition.

Discussion

350 Psychophysical experiments studying visuomotor adaptation to date mainly used one or two-
351 dimensional movement paradigms to derive theories for motor learning settings (Mazzoni and Krakauer
352 2006, Krakauer 2009, Wolpert, Diedrichsen et al. 2011, Taylor, Krakauer et al. 2014, McDougle, Bond et
353 al. 2015, Morehead, Qasim et al. 2015, Leow, de Rugy et al. 2016). Natural movement is rarely
354 constrained in this way and generalization of core theoretical concepts of motor control to
355 unconstrained three-dimensional movements has rarely been tested. Motor learning studies are
356 informative for motor rehabilitation protocols for patients that need to relearn or re-adapt existing
357 motor schemes and these patients will necessarily perform their movements in a three-dimensional
358 environment (Deutsch, Merians et al. 2004, Holden 2005, Pisella, Rode et al. 2006, Turolla, Dam et al.
359 2013). Therefore, we tested if observations and model assumptions about motor learning in one or two
360 dimensions still hold true for largely unconstrained movements in three-dimensional space. We show
361 that visuomotor adaptation under 3D stereoscopic vision depends on the plane in which a 2D
362 visuomotor rotation perturbation is applied. Subjects adapted best to perturbations in the coronal plane
363 followed by sagittal then horizontal. The rate of slow learning correlated well with the Kalman gain
364 variation across perturbation conditions, but not across subjects, as revealed by our novel hierarchical
365 Bayesian HMC modeling of the data. These results show that important aspects of OI theories of motor
366 control derived from 2D movements generalize to the largely unconstrained 3D movements studied here
367 but do not extend to the individual level for any of the applied perturbations.
368

369 **A novel two-state hierarchical HMC algorithm for precise estimation of motor learning parameters**

370 We developed a novel HMC Bayesian fitting procedure with a multilevel hierarchical structure to take
371 into account effects from multiple subjects performing a motor adaptation task in three different
372 learning conditions, i.e., different planes relative to the body were perturbed. Naturally, such a
373 hierarchical approach shows lower goodness-of-fit to single-subject adaptation curves than algorithms

374 that focus on single-subject data. But multi-subject experiments are typically designed to determine the
375 effects of experimental variations on the motor learning behavior independent of test subject. Hence, it
376 is most important to best estimate the underlying learning parameters.
377 For the current experimental design, our procedure is better able to reconstruct actual model
378 parameters than a state-of-the-art EM fitting algorithm (Albert and Shadmehr 2018) or a non-
379 hierarchical Bayesian HMC model, as revealed from the surrogate testing. This is due to the low
380 identifiability of such two-state models for relatively short adaptation experiments comprising only a few
381 dozen or even hundreds of trials per condition. The low identifiability is a result of random fluctuations
382 in the shape of the adaptation curve and are easily associated with various learning parameters (see, for
383 example, the outliers in Fig. 4). In the hierarchical model. Each parameter is sampled from a population-
384 level distribution, the parameters of which are also part of the model. This makes extreme values for the
385 reconstructed parameter less likely.
386
387 **Comparison with single-state model**
388 Using our hierarchical model, we show that a two-state model fits the data significantly better than a
389 single-state model. The two-state model is well established for subjects performing in a 2D environment
390 (Smith, Ghazizadeh et al. 2006, Wolpert, Diedrichsen et al. 2011) and better explains learning
391 mechanisms such as savings and anterograde interference in 2D settings (Huberdeau, Krakauer et al.
392 2015). As previously hypothesized (Taylor, Krakauer et al. 2014, McDougle, Bond et al. 2015), the fast
393 learning process is assumed to be associated to an explicit process and the slow learning process to an
394 implicit process, both with anatomically distinct associated brain areas (Della-Maggiore, Malfait et al.
395 2004, Shadmehr, Smith et al. 2010, Taylor, Krakauer et al. 2014). While it is plausible to assume that an
396 interplay of explicit and implicit learning mechanisms is independent of the dimensionality of the task, to
397 our knowledge, the two-state model to date has not been demonstrated for adaptation paradigms

398 involving 3D movements. The fact that, in a 3D setting, we found a two-state model to better fit the
399 adaptation data than a single-state model without introducing paradigms that manipulate explicit
400 learning mechanisms (like withholding the visual feedback (Wei and Kording 2010)), might indicate that
401 the explicit learning component in our three dimensional-paradigm is more pronounced than in classic
402 two-dimensional paradigms.
403
404 **Differences in planning and measurement noises are related to learning rate**
405 Differences in the slow and fast learning rates between the planes are associated with different
406 adaptation levels in our data. The coronal plane yielded the lowest measurement noise and subjects
407 adapted fastest to perturbations (Fig.5B). It is important to note that in our model, this measurement
408 noise represents the reliability of the subject measurements of the cursor position. This is likely due to
409 the fact that in our setup, subjects have to rely mainly on visual stereoscopy to estimate depth. Visual
410 localization is less precise in depth (van Beers, Wolpert et al. 2002, Gepshtein and Banks 2003) and
411 depth is not perturbed by a rotation in the coronal plane. On the other hand, rotations in the sagittal and
412 horizontal plane both resulted in cursor depth changes compared to baseline. Indeed, other studies also
413 showed that subjects tend to adapt worse when the sensory noise was increased by practically blurring
414 the error feedback (Kording and Wolpert 2004, Burge, Ernst et al. 2008, Wei and Kording 2010).
415 However, not all differences in the final adaptation or learning rates levels can simply be explained by
416 perceptual differences: we also found that perturbations in the horizontal plane were the most difficult
417 to learn, despite having measurement variability levels close to those of the coronal plane (Fig 5B-
418 measurement variability). In horizontal perturbations, subjects show the lowest level of planning
419 variability (Fig5B-planning variability). This could potentially be explained in our experiment by the
420 observation that in everyday life, humans tend to perform precise visually-guided upper-limb movement
421 more frequently in the horizontal plane (writing, typing, cooking). Our findings agree with other studies

that found that subjects adapt faster when state estimation uncertainty is increased (Burge, Ernst et al. 2008, Wei and Kording 2010).

When looking at all three planes of perturbation, the learning rate cannot be explained by the measurement noise only or the planning noise only or by a linear combination of the two.

Optimal integration theory in 3D

Previous studies (Burge, Ernst et al. 2008, van Beers 2009, Wei and Kording 2010, He, Liang et al. 2016, van der Vliet, Frens et al. 2018), provided evidence for the OI theory during visuomotor adaptation. They showed that the planning component of motor noise correlates positively with the adaptation rate while the measurement component correlates negatively, at least when the respective noise component experimentally is kept constant. While the adaptation data from our 3D movements yielded similar trends, the correlation of slow learning rate with either measurement- or planning-variability was weak. For an optimal learner, the Kalman gain is indicative of the level of correction attributed to the experienced error (Burge, Ernst et al. 2008, Wei and Kording 2010, He, Liang et al. 2016). This Kalman gain positively correlates with the slow learning rate in our data, supporting the idea that subjects optimally integrate the information relative to the internal state with experienced (visual) feedback. However, and as opposed to what was suggested in previous studies (He, Liang et al. 2016, van der Vliet, Frens et al. 2018), we observe the correlation between Kalman gain and slow learning rate only across different perturbation conditions. Within each perturbation condition, there was no relationship between Kalman gain and slow learning rate at the subject population level.

Conclusion

Here, we develop a novel HMC fitting procedure to correlate learning rates and noise levels estimated with the same model and without the need to experimentally manipulating these error variabilities. By

applying this model to a sensorimotor adaptation task in 3D, we found that the rate of adaptation with which subjects counteract applied visuomotor rotations, depends on the statistics of the combined errors with which subjects plan and perceived movements, and these differ between different axes relative to the body. This insight could be used in motor rehabilitation strategies by specifically targeting the orientation of the body relative to the target while performing reaching movements to accelerate learning.

Funding:

German Research Foundation (DFG, Germany, grant number FOR-1847-GA1475-B2). Received by AG.

German Research Foundation (DFG, Germany, grant number SFB-889). Received by AG.

Federal Ministry for Education and Research (BMBF, Germany, grant number 01GQ1005C). Received by AG.

Figure Captions

Fig 1. A) Schematic representation of our virtual reality setup. The two angled mirrors reflect the image from the two screens to the two eyes independently providing stereoscopic vision. The mirrors are semitransparent to allow calibration of the virtual reality space with the real hand position. During the experiments they were obscured from so that the subjects were not seeing the robotic manipulator or their real hand but only the cursor overlapped it. B) Temporal structure of the task. Following a brief holding period, the subject had to reach to one of eight targets arranged at the edges of a cube. The cube is orientated relatively to the tilted head of the subject and workspace and not according to true horizontal and vertical. C) The subjects reached from the center of the cube to one of the eight targets. Here all baseline trajectories are simultaneously displayed. D) Temporal structure of each of the three perturbation experiments. Following a baseline phase of 120 trials, a classical visuomotor perturbation was applied for 240 trials followed by a washout of 240 additional trials. The rotation coordinate system and the type of rotation are visualized below. The perturbation type was always a 30 degrees rotation of the cursor around the sagittal, coronal or horizontal plane depending on the block. In the figure a rotation in the horizontal plane is represented.

Fig 2. A) Example trajectories from one subject. Each row/color of the graph correspond to different directions of rotations. The trajectories are projected on the plane perpendicular of the axis of rotation for representation and analysis. The plot shows similarities across these trajectories when projected in

the plane of the applied perturbation. B) Transformation of the trajectories in the task relevant dimensions (perturbed dimension and center to target dimension). To compare data across tasks each trajectory was resampled and transformed in the new reference frame. At half of the trajectory the adaptation angle was calculated from the transformed dimensions and used for model fitting.C) examples of transformed trajectories from one subject during baseline, early adaptation and late adaptation

Fig 3. A) Final adaptation level for each plane. B) Examples of data fitted with one-state and two-states learning models. Black points represent the subject's data (average of angles at half-trajectory angle within 8-trial epochs) and the black dashed line the perturbation profile. Blue line: Single-state model. Orange line: two-state model (sum of the fast- and slow-states). Red lines: slow-state from the two-state model. Green lines: fast-state from the two-state model. C) Histogram of the RMSE values for all adaptation profiles (error between the actual data and the noiseless adaptation profiles) with the one-state and the two-states models.

Fig 4. Comparison of parameter estimation quality between our HMC hierarchical fitting procedure (orange), an HMC non-hierarchical fitting procedure (red) and a EM fitting procedure ((Albert and Shadmehr 2018) EM, blue). For each model parameter in randomly drawn two-state models we represent the error in parameter reconstruction (estimated parameter – drawn parameter) for each fitting procedure: histogram of the absolute error and average and 95% confidence intervals of the squared error. We also represent the correlation (average and 95%CI) between the estimated and drawn parameters.

Fig 5. Comparison of two-state model parameters between the perturbation planes. A) The colored lines represent the model parameter values obtained for all subjects (one line/color per subject : $\sigma_{u,jp}$, $a_{s,jp}$, $a_{f,jp}$, $b_{s,jp}$, $b_{f,jp}$, $\sigma_{x,jp}$) for the different perturbation planes. The error bars correspond to 95 % credible intervals (i.e. contain 95% of the posterior probability) for the population average hyper-parameters $\mu_{a_s,p}$, $\mu_{a_f,p}$, $\mu_{b_s,p}$, $\mu_{b_f,p}$, $\mu_{\sigma_x,p}$, $\mu_{\sigma_u,p}$. The steady-state Kalman gain K was computed from the posteriors of the measurement noise and planning noise. B) Relationships between the slow learning rate Bs and uncertainty related parameters: measurement noise variance, planning noise variance, and steady-state Kalman gain. Points correspond to individual subjects' parameters in the different rotation planes (coded by color). The correspondingly colored lines represent linear fits based on the subjects' parameter values within each plane. The grey line corresponds to a linear fit based on subjects' parameter values across all planes. The horizontal and vertical error bars correspond to 95 % credible intervals for the corresponding parameter population average hyper-parameters.

References

Albert, S. T. and R. Shadmehr (2018). "Estimating properties of the fast and slow adaptive processes during sensorimotor adaptation." J Neurophysiol **119**(4): 1367-1393.

Anglin, J. M., T. Sugiyama and S. L. Liew (2017). "Visuomotor adaptation in head-mounted virtual reality versus conventional training." Sci Rep **7**: 45469.

Avraham, G., J. R. Morehead, H. E. Kim and R. B. Ivry (2020). "Re-exposure to a sensorimotor perturbation produces opposite effects on explicit and implicit learning processes." bioRxiv.

Baddeley, R. J., H. A. Ingram and R. C. Miall (2003). "System identification applied to a visuomotor task: near-optimal human performance in a noisy changing task." J Neurosci **23**(7): 3066-3075.

Burge, J., M. O. Ernst and M. S. Banks (2008). "The statistical determinants of adaptation rate in human reaching." J Vis **8**(4): 20 21-19.

Cheng, S. and P. N. Sabes (2006). "Modeling sensorimotor learning with linear dynamical systems." Neural Comput **18**(4): 760-793.

Cheng, S. and P. N. Sabes (2007). "Calibration of visually guided reaching is driven by error-corrective learning and internal dynamics." J Neurophysiol **97**(4): 3057-3069.

Choi, W., J. Lee, N. Yanagihara, L. Li and J. Kim (2018). "Development of a quantitative evaluation system for visuo-motor control in three-dimensional virtual reality space." Sci Rep **8**(1): 13439.

Della-Maggiore, V., N. Malfait, D. J. Ostry and T. Paus (2004). "Stimulation of the posterior parietal cortex interferes with arm trajectory adjustments during the learning of new dynamics." J Neurosci **24**(44): 9971-9976.

Deutsch, J. E., A. S. Merians, S. Adamovich, H. Poizner and G. C. Burdea (2004). "Development and application of virtual reality technology to improve hand use and gait of individuals post-stroke." Restor Neurol Neurosci **22**(3-5): 371-386.

Diedrichsen, J., R. Shadmehr and R. B. Ivry (2010). "The coordination of movement: optimal feedback control and beyond." Trends Cogn Sci **14**(1): 31-39.

Ernst, M. O. and M. S. Banks (2002). "Humans integrate visual and haptic information in a statistically optimal fashion." Nature **415**(6870): 429-433.

Friston, K. (2011). "What is optimal about motor control?" Neuron **72**(3): 488-498.

Gelman, A. (2006). "Prior distributions for variance parameters in hierarchical models (comment on article by Browne and Draper)." Bayesian analysis **1**(3): 515-534.

Gelman, A., D. Lee and J. Guo (2015). "Stan: A probabilistic programming language for Bayesian inference and optimization." Journal of Educational and Behavioral Statistics **40**(5): 530-543.

Gepshtein, S. and M. S. Banks (2003). "Viewing geometry determines how vision and haptics combine in size perception." Curr Biol **13**(6): 483-488.

Ghahramani, Z., D. M. Wolpert and M. I. Jordan (1997). Computational models of sensorimotor integration. Advances in Psychology. P. Morasso and V. Sanguineti, North-Holland. **119:** 117-147.

He, K., Y. Liang, F. Abdollahi, M. Fisher Bittmann, K. Kording and K. Wei (2016). "The Statistical Determinants of the Speed of Motor Learning." PLoS Comput Biol **12**(9): e1005023.

Hoffman, M. D. and A. Gelman (2014). "The No-U-Turn sampler: adaptively setting path lengths in Hamiltonian Monte Carlo." J. Mach. Learn. Res. **15**(1): 1593-1623.

Holden, M. K. (2005). "Virtual environments for motor rehabilitation: review." Cyberpsychol Behav **8**(3): 187-211; discussion 212-189.
Huang, V. S., A. Haith, P. Mazzoni and J. W. Krakauer (2011). "Rethinking motor learning and savings in adaptation paradigms: model-free memory for successful actions combines with internal models." Neuron **70**(4): 787-801.
Huberdeau, D. M., J. W. Krakauer and A. M. Haith (2015). "Dual-process decomposition in human sensorimotor adaptation." Curr Opin Neurobiol **33**: 71-77.
Inoue, M. and S. Kitazawa (2018). "Motor Error in Parietal Area 5 and Target Error in Area 7 Drive Distinctive Adaptation in Reaching." Curr Biol **28**(14): 2250-2262 e2253.
Kalman, R. E. (1960). "A New Approach to Linear Filtering and Prediction Problems." Journal of Basic Engineering **82**(1): 35-45.
Kording, K. P. and D. M. Wolpert (2004). "Bayesian integration in sensorimotor learning." Nature **427**(6971): 244-247.
Korenberg, A. and Z. Ghahramani (2002). "A Bayesian view of motor adaptation." Cahiers de Psychologie Cognitive **21**.
Krakauer, J. W. (2009). "Motor learning and consolidation: the case of visuomotor rotation." Adv Exp Med Biol **629**: 405-421.
Krakauer, J. W., C. Ghez and M. F. Ghilardi (2005). "Adaptation to visuomotor transformations: consolidation, interference, and forgetting." J Neurosci **25**(2): 473-478.
Leow, L. A., A. de Rugy, W. Marinovic, S. Riek and T. J. Carroll (2016). "Savings for visuomotor adaptation require prior history of error, not prior repetition of successful actions." J Neurophysiol **116**(4): 1603-1614.
Mazzoni, P. and J. W. Krakauer (2006). "An implicit plan overrides an explicit strategy during visuomotor adaptation." J Neurosci **26**(14): 3642-3645.
McDougle, S. D., K. M. Bond and J. A. Taylor (2015). "Explicit and Implicit Processes Constitute the Fast and Slow Processes of Sensorimotor Learning." J Neurosci **35**(26): 9568-9579.
Morehead, J. R., S. E. Qasim, M. J. Crossley and R. Ivry (2015). "Savings upon Re-Aiming in Visuomotor Adaptation." J Neurosci **35**(42): 14386-14396.
Morel, P. (2018). "Gramm: grammar of graphics plotting in Matlab." The Journal of Open Source Software **3**(23).
Morel, P. D. and P. Baraduc (2010). Dissociating the impact of sensory and motor noise in human saccades. Cinquième conférence plénière française de Neurosciences Computationnelles, "Neurocomp'10". Lyon, France.
Pisella, L., G. Rode, A. Farne, C. Tilikete and Y. Rossetti (2006). "Prism adaptation in the rehabilitation of patients with visuo-spatial cognitive disorders." Curr Opin Neurol **19**(6): 534-542.
Rosenberg, L. (1993). The effect of interocular distance upon operator performance using stereoscopic displays to perform virtual depth tasks.
Scott, S. H. (2004). "Optimal feedback control and the neural basis of volitional motor control." Nat Rev Neurosci **5**(7): 532-546.
Shadmehr, R. and J. W. Krakauer (2008). "A computational neuroanatomy for motor control." Exp Brain Res **185**(3): 359-381.
Shadmehr, R., M. A. Smith and J. W. Krakauer (2010). "Error correction, sensory prediction, and adaptation in motor control." Annu Rev Neurosci **33**: 89-108.
Sing, G. C. and M. A. Smith (2010). "Reduction in learning rates associated with anterograde interference results from interactions between different timescales in motor adaptation." PLoS Comput Biol **6**(8).
Smith, M. A., A. Ghazizadeh and R. Shadmehr (2006). "Interacting adaptive processes with different timescales underlie short-term motor learning." PLoS Biol **4**(6): e179.

Taylor, J. A., J. W. Krakauer and R. B. Ivry (2014). "Explicit and implicit contributions to learning in a sensorimotor adaptation task." J Neurosci **34**(8): 3023-3032.
Turolla, A., M. Dam, L. Ventura, P. Tonin, M. Agostini, C. Zucconi, P. Kiper, A. Cagnin and L. Piron (2013). "Virtual reality for the rehabilitation of the upper limb motor function after stroke: a prospective controlled trial." J Neuroeng Rehabil **10**: 85.
van Beers, R. J. (2009). "Motor learning is optimally tuned to the properties of motor noise." Neuron **63**(3): 406-417.
van Beers, R. J., P. Baraduc and D. M. Wolpert (2002). "Role of uncertainty in sensorimotor control." Philos Trans R Soc Lond B Biol Sci **357**(1424): 1137-1145.
van Beers, R. J., A. C. Sittig and J. J. Gon (1999). "Integration of proprioceptive and visual position-information: An experimentally supported model." J Neurophysiol **81**(3): 1355-1364.
van Beers, R. J., D. M. Wolpert and P. Haggard (2002). "When feeling is more important than seeing in sensorimotor adaptation." Curr Biol **12**(10): 834-837.
van der Vliet, R., M. A. Frens, L. de Vreede, Z. D. Jonker, G. M. Ribbers, R. W. Selles, J. N. van der Geest and O. Donchin (2018). "Individual Differences in Motor Noise and Adaptation Rate Are Optimally Related." eNeuro **5**(4).
Vehtari, A., A. Gelman and J. Gabry (2017). "Practical Bayesian model evaluation using leave-one-out cross-validation and WAIC." Statistics and computing **27**(5): 1413-1432.
Wei, K. and K. Kording (2010). "Uncertainty of feedback and state estimation determines the speed of motor adaptation." Front Comput Neurosci **4**: 11.
Wolpert, D. M., J. Diedrichsen and J. R. Flanagan (2011). "Principles of sensorimotor learning." Nat Rev Neurosci **12**(12): 739-751.
Wolpert, D. M. and Z. Ghahramani (2000). "Computational principles of movement neuroscience." Nat Neurosci **3 Suppl**: 1212-1217.

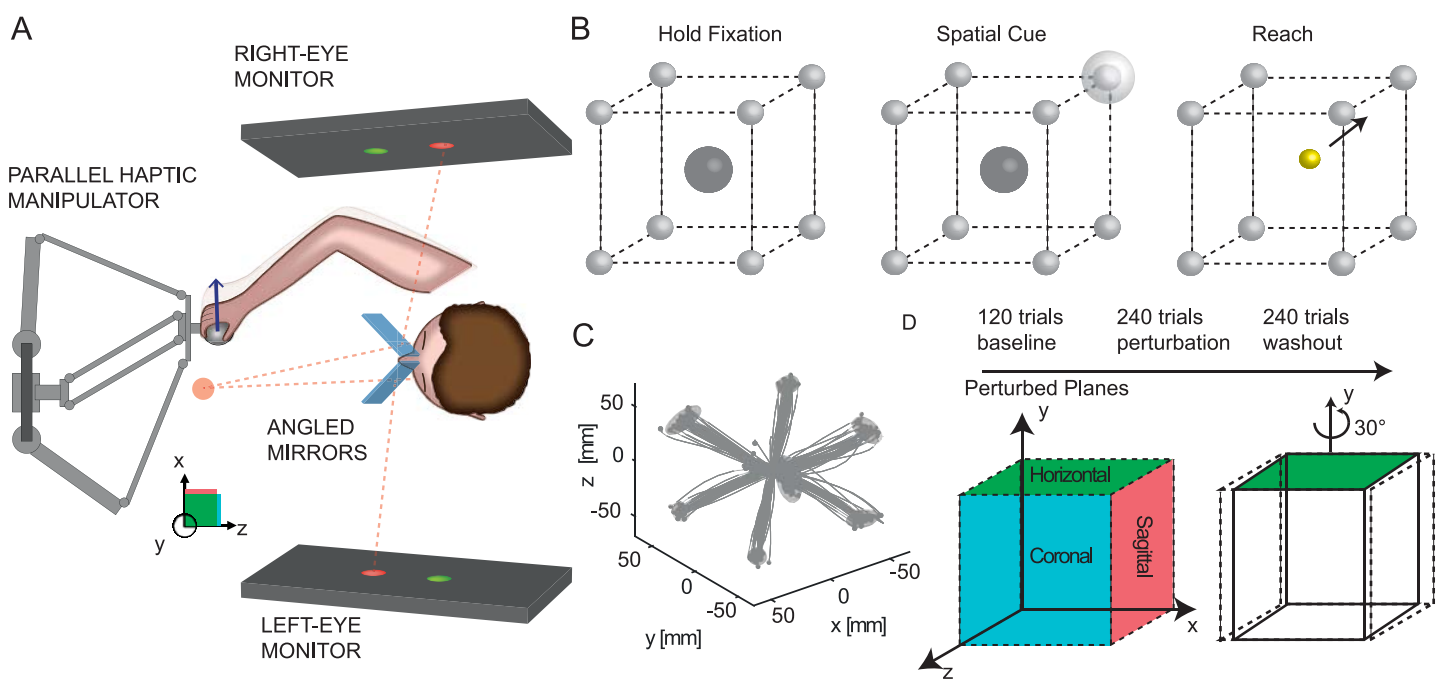
A
RIGHT-EYE MONITOR
PARALLEL HAPTIC MANIPULATOR
ANGLED MIRRORS
LEFT-EYE MONITOR
x
y
z
B
Hold Fixation
Spatial Cue
Reach
C
z [mm]
50
0
-50
y [mm]
x [mm]
D
120 trials baseline
240 trials perturbation
240 trials washout
Perturbed Planes
Horizontal
Coronal
Sagittal
30°

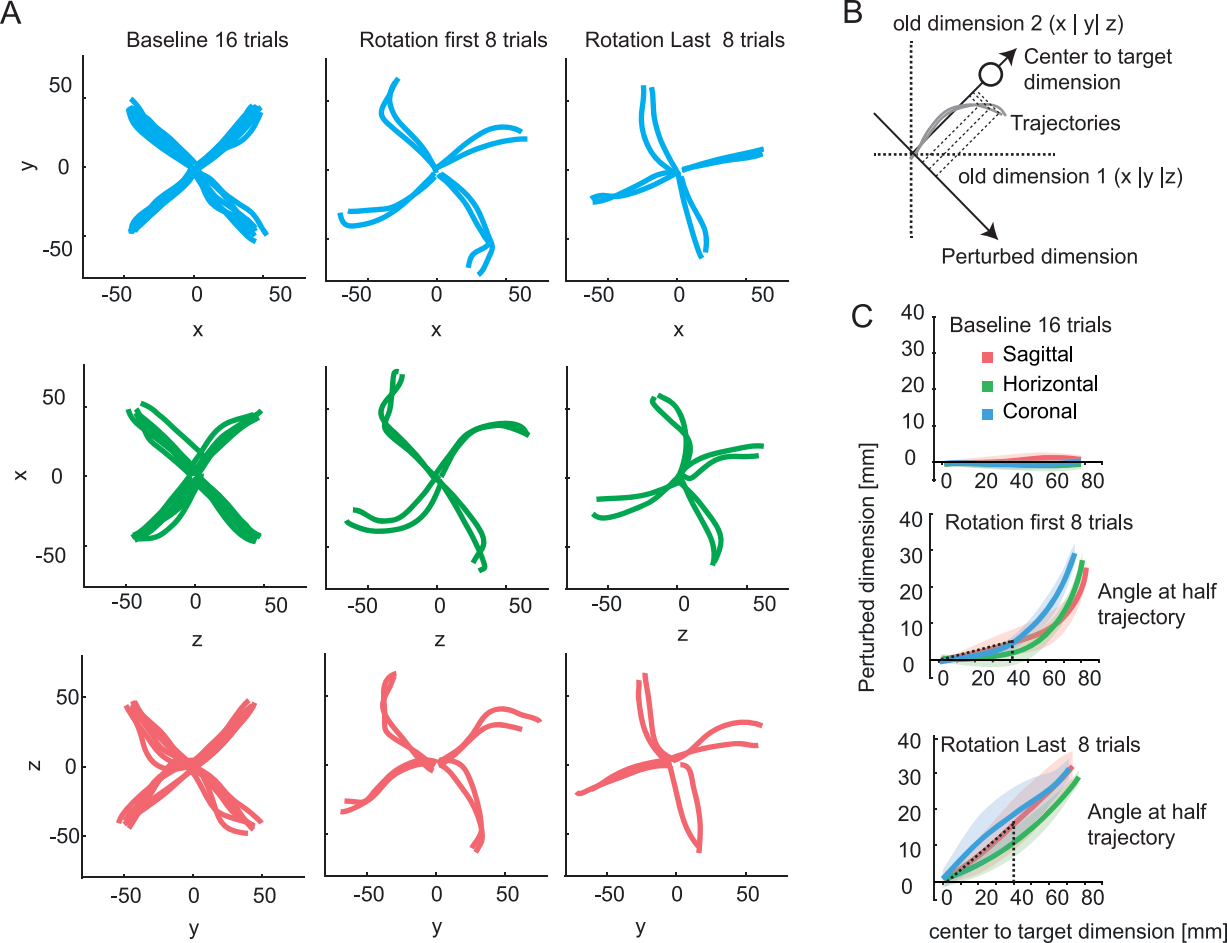
A
Baseline 16 trials
Rotation first 8 trials
Rotation Last 8 trials
y
x
z
B
old dimension 2 (x | y| z)
Center to target dimension
Trajectories
old dimension 1 (x |y |z)
Perturbed dimension
C
Baseline 16 trials
Sagittal
Horizontal
Coronal
Rotation first 8 trials
Angle at half trajectory
Rotation Last 8 trials
Perturbed dimension [mm]
center to target dimension [mm]

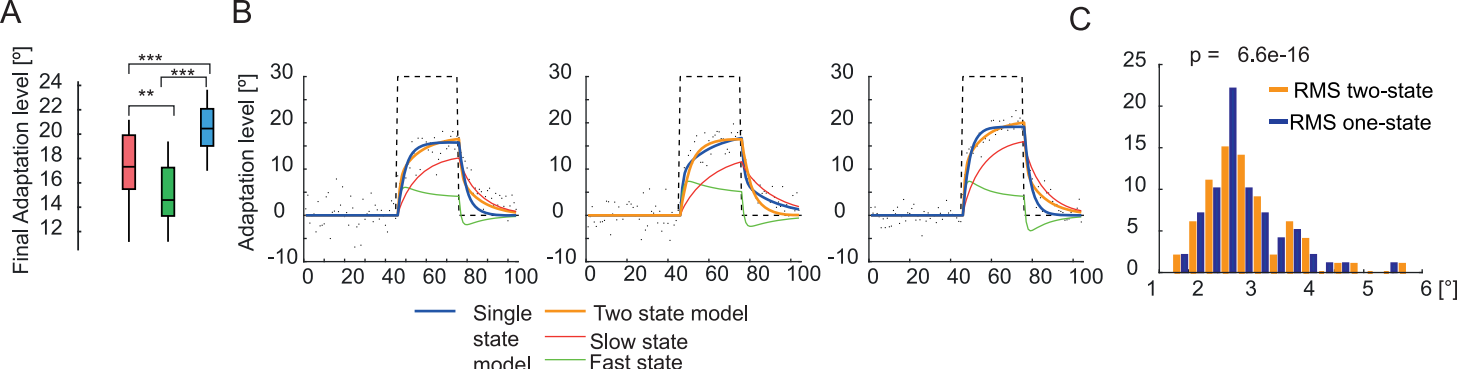
A
Final Adaptation level [°]
24
22
20
18
16
14
12
***
***
**
B
Adaptation level [°]
30
20
10
0
-10
0
20
40
60
80
100
Single state model
Two state model
Slow state
Fast state
C
p = 6.6e-16
RMS two-state
RMS one-state
25
20
15
10
5
0
1
2
3
4
5
6 [°]

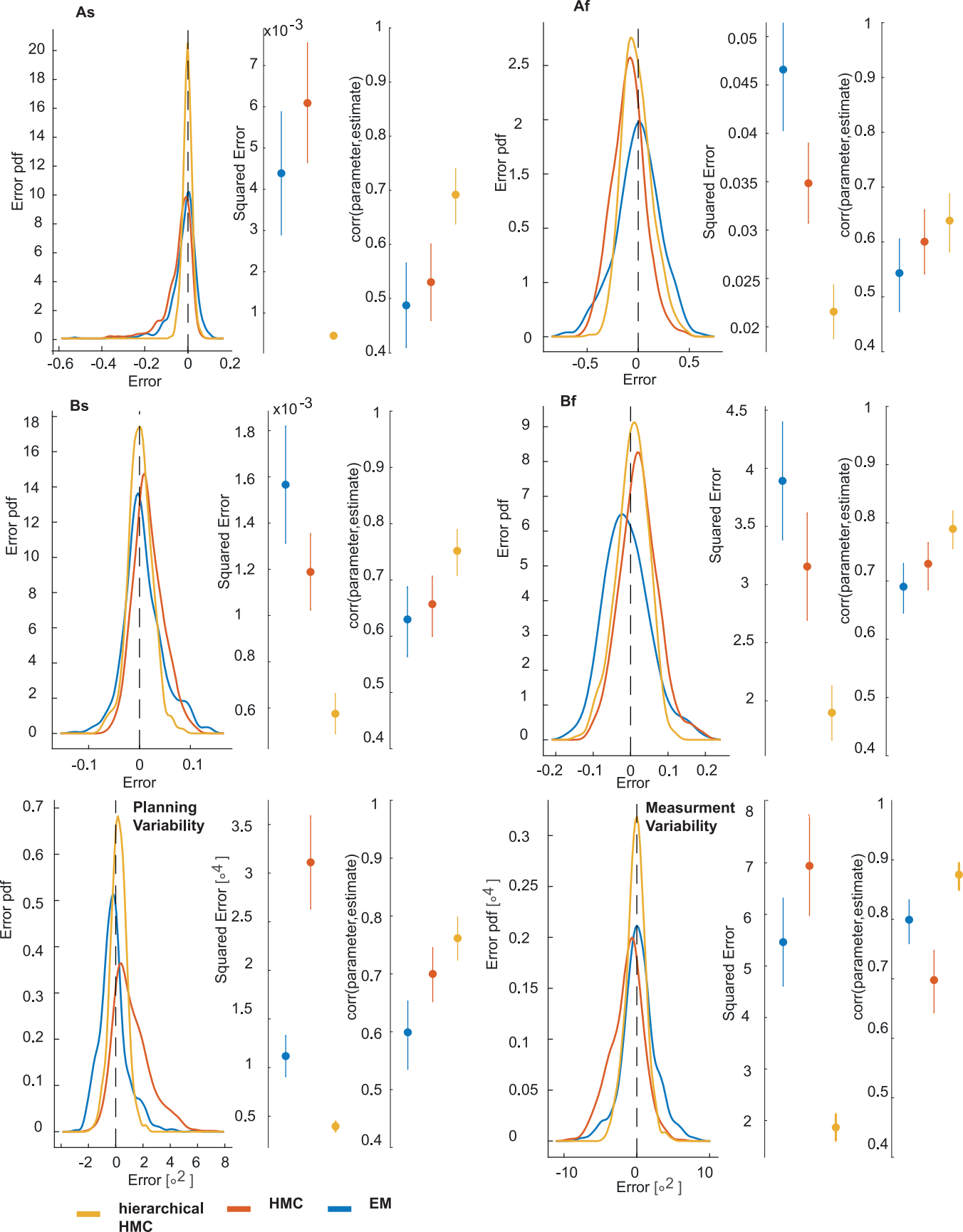
As
Af
Bs
Bf
Planning Variability
Measurment Variability
Error pdf
Error
Squared Error
x10^-3
corr(parameter,estimate)
Error pdf [∘^4]
Squared Error [∘^4]
Error [∘^2]
hierarchical HMC
HMC
EM

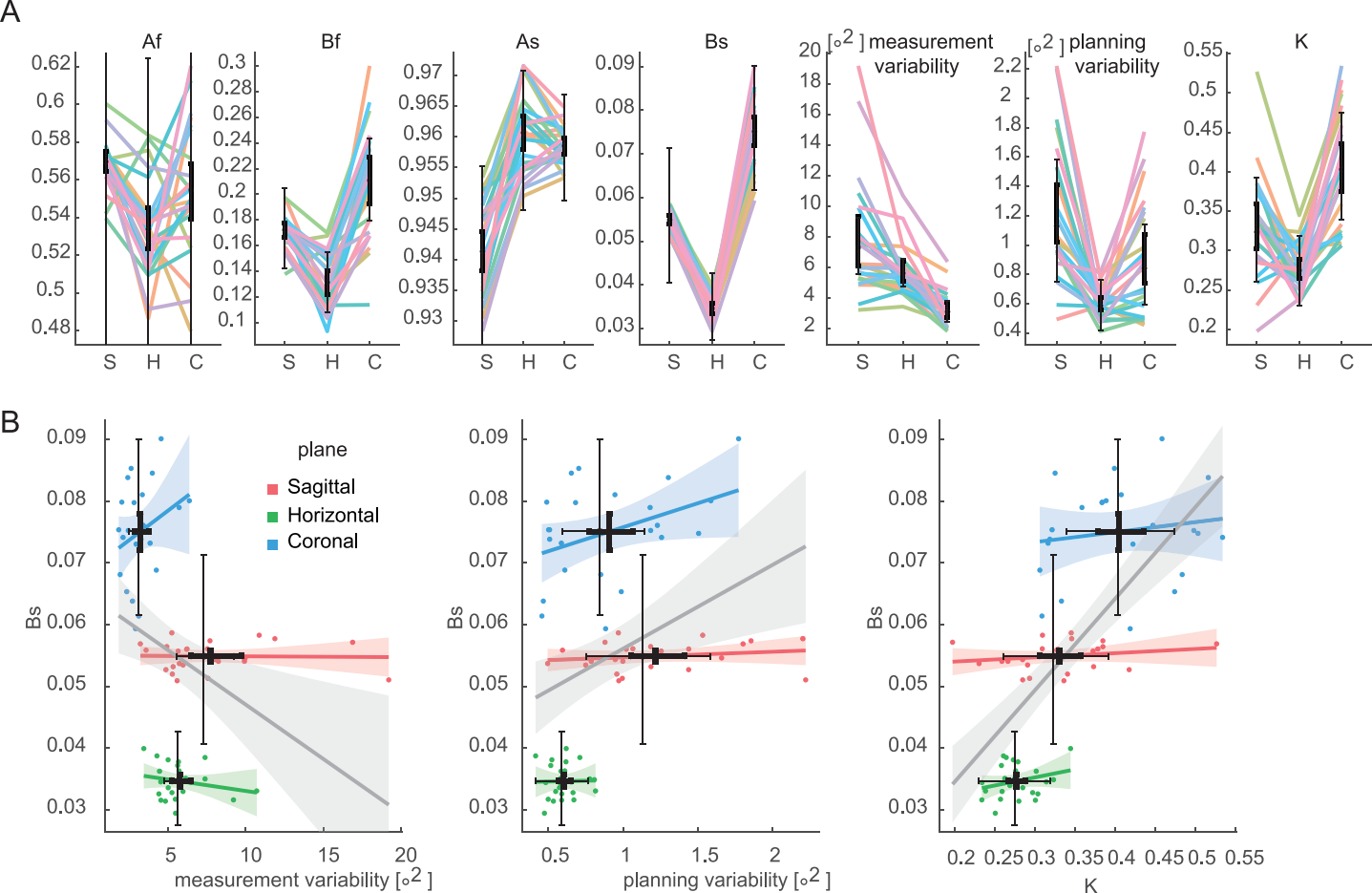
A
Af
Bf
As
Bs
[∘2] measurement variability
[∘2] planning variability
K
S H C
B
plane
Sagittal
Horizontal
Coronal
Bs
measurement variability [∘2]
planning variability [∘2]
K